Molecular identification by generating coherence between molecular normal modes using stimulated Raman scattering

Daniel L. Marks,[1] Joseph B. Geddes III,[1] and Stephen A. Boppart[1,2,*]

[1]Beckman Institute for Advanced Science and Technology, Department of Electrical and Computer Engineering, University of Illinois at Urbana-Champaign, Urbana, Illinois 61801, USA
[2]Department of Bioengineering and the Department of Internal Medicine, the College of Engineering, and the College of Medicine, University of Illinois at Urbana-Champaign, Urbana, Illinois 61801, USA
*Corresponding author: boppart@illinois.edu

Received October 31, 2008; revised January 16, 2009; accepted February 10, 2009; posted April 27, 2009 (Doc. ID 103524); published June 2, 2009

We propose a method of driving the vibrations of normal modes of a target molecule into coherence using stimulated Raman scattering. In concert many vibrations can produce a larger anti-Stokes signal than a single vibration. The same illumination does not drive other molecules to have coherent vibrations so that these molecules produce a weaker signal. We investigate how target and confounder molecules can be distinguished by pulses that drive many vibrations coherently, which has applications in coherent Raman microspectroscopy. © 2009 Optical Society of America

OCIS codes: 300.6450, 170.5660, 190.5650.

The Raman spectroscopy of biological tissues is extremely challenging owing to the highly heterogeneous content. Methods such as coherent anti-Stokes Raman scattering (CARS) microscopy [1,2] and nonlinear interferometric vibrational imaging [3–6] probe the vibrational spectra of molecular normal modes but are not specific to particular molecules. Rather than attempting to interpret complex Raman spectra, it may be more desirable to engineer electromagnetic radiation that produces a signal selectively from molecules of interest. We describe an electromagnetic pulse that, through stimulated Raman scattering (SRS), maximizes the coherence between vibrations of normal modes in the target molecule. Induced coherent vibrations radiate anti-Stokes Raman radiation constructively, producing a larger and more specific signal for a particular molecule than would be generated by a single vibration.

Equations (1) and (2) model the two SRS processes that describe the anti-Stokes radiation spectrum $\tilde{P}^{(3)}(\omega)$ of a point-scatterer CARS process [7,8]. The incident electric field is given by $E(t)$ and contains no frequencies directly resonant with the scatterer medium. The spectrum of the complex analytic signal of $E(t)$ is $\tilde{E}(\omega)$ such that $E(t)=\pi^{-1}\mathrm{Re}\{\int_0^\infty \mathrm{d}\omega \exp(i\omega t)\times\tilde{E}(\omega)\}$.The Raman susceptibility of the scatterer is $\tilde{\chi}^{(3)}(\Omega)$, where Ω is a vibrational frequency. Uncoupled normal modes are assumed:

$$\tilde{Q}(\Omega)=\tilde{\chi}^{(3)}(\Omega)\int_0^\infty \tilde{E}(\omega+\Omega)\tilde{E}(\omega)^*\mathrm{d}\omega, \tag{1}$$

$$\tilde{P}^{(3)}(\omega)=\int_0^\omega \tilde{E}(\omega-\Omega)\tilde{Q}(\Omega)\mathrm{d}\Omega. \tag{2}$$

The first SRS process of Eq. (1) induces oscillations in the medium with total amplitude $\tilde{Q}(\Omega)$. The second SRS process of Eq. (2) models the anti-Stokes emission $\tilde{P}^{(3)}(\omega)$. Equation (1) is expressed in the time domain using $Q(t)=\pi^{-1}\mathrm{Re}\{\int_0^\infty \mathrm{d}\Omega \exp(i\Omega t)\tilde{Q}(\Omega)\}$ and $\chi^{(3)}(t)=\pi^{-1}\mathrm{Re}\{\int_0^\infty \mathrm{d}\Omega \exp(i\Omega t)\tilde{\chi}^{(3)}(\Omega)\}$:

$$Q(t)=\int_{-\infty}^{\infty}\mathrm{d}t'|E(t-t')|^2\chi^{(3)}(t'). \tag{3}$$

This equation is the convolution of the instantaneous intensity of the electric field $|E(t)|^2$ and a Raman impulse response $\chi^{(3)}(t)$. A typical Raman scattering experiment is modeled by an illumination of monochromatic waves $E(t)=E_0\cos(\omega_1 t)+E_0\cos(\omega_2 t)$. These waves excite an oscillation $Q(t)=(E_0^2/2)\mathrm{Re}\{\tilde{\chi}^{(3)}(\Omega)\times\exp(i\Omega t)\}$, and the vibrational frequency $\Omega=|\omega_1-\omega_2|$ is probed.

Rather than this scheme, a matched pulse illuminates the scatterer such that $|E(t)|^2\propto\chi^{(3)}(-t)$, which resembles the time-reversed Raman impulse response. $Q(t)$ is then proportional to the autocorrelation of $\chi^{(3)}(t)$, with its maximum value at $t=0$ when all of the vibrations are excited constructively. At time $t=0$, other molecules' normal modes are not in phase and generate a weaker anti-Stokes signal. This "matched pulse" idea derives from a concept in communications theory, the matched filter [9], because Eq. (3) is a linear, time-invariant system driven by the envelope $|E(t)|^2$.

To design a pulse field $E(t)$ with a given envelope $|E(t)|^2\propto A(t)$, the following method is proposed. The envelope $A(t)\geq 0$ for $-t_m\leq t\leq 0$ and $A(t)=0$ otherwise, where t_m is the maximum delay manipulated by the pulse-shaping apparatus [10]. The pulse spectrum is constrained to $|\tilde{E}(\omega)|^2\leq S(\omega)$, where $S(\omega)$ is the source spectrum. The following iterative method was implemented to find successive electric-field iterations $\tilde{E}^{(n)}(\omega)$:

0146-9592/09/121756-3/$15.00

1. Start with a random guess for $\tilde{E}^{(0)}(\omega)$ such that $|\tilde{E}^{(0)}(\omega)| = \sqrt{S(\omega)}$ but has a random phase.
2. Transform to the time domain such that $E^{(n)}(t) = (2\pi)^{-1}\int_0^\infty \mathrm{d}\omega \exp(i\omega t)\tilde{E}^{(n-1)}(\omega)$.
3. Enforce the time-domain amplitude constraint by computing $\hat{E}^{(n)}(t) = (1-\alpha)E^{(n)}(t) + \alpha\sqrt{A(t)}(E^{(n)}(t)/|E^{(n)}(t)|)\sqrt{\int_{-\infty}^{\infty}\mathrm{d}t'|E^{(n)}(t')|^2/\int_{-\infty}^{\infty}\mathrm{d}t'|A(t')|}$ with $0<\alpha<1$ being a relaxation constant to stabilize the iterations.
4. Transform to the frequency domain such that $\hat{\tilde{E}}^{(n)}(\omega) = \int_{-\infty}^{\infty}\mathrm{d}t \exp(-i\omega t)\hat{E}^{(n)}(t)$.
5. Enforce the constraint $|\tilde{E}(\omega)| < \sqrt{S(\omega)}$ by computing $\tilde{\epsilon}^{(n)}(\omega) = \hat{\tilde{E}}^{(n)}(\omega)\sqrt{S(\omega)}/|\hat{\tilde{E}}^{(n)}(\omega)|$ for $|\hat{\tilde{E}}^{(n)}(\omega)| > \sqrt{S(\omega)}$ and $\tilde{\epsilon}^{(n)}(\omega) = \hat{\tilde{E}}^{(n)}(\omega)$ otherwise.
6. Relax the iteration by setting $\tilde{E}^{(n)}(\omega) = (1-\beta)\tilde{E}^{(n-1)}(\omega) + \beta\tilde{\epsilon}^{(n)}(\omega)$ for $0<\beta<1$.
7. Continue at step 2 until insignificant changes to $\tilde{E}^{(n)}(\omega)$ occur between iterations.

The fast Fourier transform implements the Fourier integrals on discrete spectra. The choice of $\alpha = 0.4$ and $\beta = 0.2$ appears to ensure reliable convergence.

In practice $|E(t)|^2$ is nonnegative, while $\chi^{(3)}(t)$ may be negative. A nonnegative approximation $A(t)$ for $\chi^{(3)}(t)$ is made that efficiently utilizes the source spectrum:

$$W(t) = \sqrt{\frac{\gamma^2}{w}\int_{t-w/2}^{t+w/2}\mathrm{d}t'|\chi^{(3)}(t')|^2}, \tag{4}$$

so that

$$A'(t) = \chi^{(3)}(t) + W(t), \tag{5}$$

where

$$A(t) = A'(-t) \text{ for } A'(-t) > 0 \text{ and } -t_m \leq t \leq 0, \tag{6}$$

and

$$A(t) = 0 \text{ otherwise}. \tag{7}$$

Positivity of $A(t)$ is enforced by adding a positive $W(t)$ to $\chi^{(3)}(t)$, while negative $A(t)$ are set to zero. The parameter γ trades fidelity of the impulse response with efficiency at exciting the target molecule. This pulse design may not be optimal for maximizing signal from a molecule or for discriminating between molecules, but it accounts for the essential compromises.

Figure 1 details a matched-filter Raman spectroscopy instrument. A Raman-active medium generating anti-Stokes radiation is present in one arm of a Mach–Zehnder interferometer. The source produces the bandwidth for both the excitation and reference pulses. The excitation bandwidth is shaped to form a pulse with a spectrum $\tilde{E}(\omega)$. A reference field of spectrum $\tilde{R}(\omega)$ with bandwidth coinciding with the anti-Stokes radiation is interfered with the anti-Stokes radiation. A dichroic beam splitter separates the excitation and reference pulses. The Raman medium, with a susceptibility $\tilde{\chi}^{(3)}(\Omega)$, oscillates with an anti-Stokes polarization $\tilde{P}^{(3)}(\omega)$ as per Eqs. (1) and (2). A high-pass filter separates the medium anti-Stokes frequencies and the excitation. At the second beam splitter, the reference field and the anti-Stokes field are interfered and detected at two dual-balanced photodetectors. The difference in intensity $\Delta I(\Delta t)$ captured by the photodetectors given a relative delay Δt is

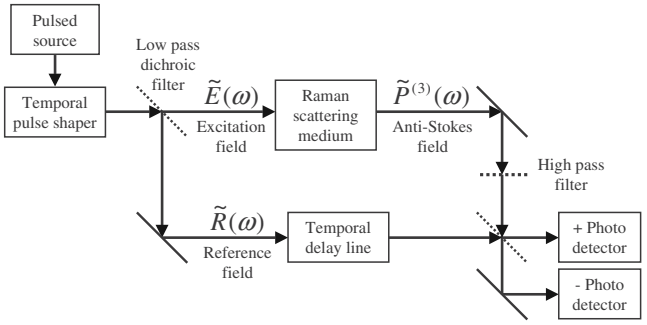

Fig. 1. Schematic of a matched-filter Raman imaging instrument that implements the matched-filter Raman spectroscopy method.

$$\Delta I(\Delta t) = 4\,\mathrm{Re}\left\{\int_0^\infty \mathrm{d}\omega \tilde{R}(\omega)\tilde{P}^{(3)}(\omega)^* \exp(-i\omega\Delta t)\right\}. \tag{8}$$

The cross correlation between the fields is sampled as the delay Δt is scanned. If the reference field $\tilde{R}(\omega) \propto \tilde{P}^{(3)}(\omega)$, the interference signal is the autocorrelation of the anti-Stokes field. By shaping the reference field to match the anti-Stokes field, the interference signal at $\Delta t = 0$ is a matched filter for the emitted anti-Stokes field of a molecule.

A simulation was performed including a target molecule and two confounders. The target molecule spectrum consisted of four equal-magnitude Lorentzian lines at 700, 1000, 1250, and 1450 cm^{-1}, each with a 10 cm^{-1} resonance width. Confounder A (CA) had frequencies of 900, 1100, and 1350 cm^{-1} each of 10 cm^{-1} width, with none in common with the target. Confounder B (CB) had frequencies of 800, 1000, and 1450 cm^{-1} each of 10 cm^{-1} width, with two in common with the target. CB has more overlap with the target than would be expected between most molecules and therefore is an exceptionally difficult scenario. The source spectrum is Gaussian with a center frequency of 12,500 cm^{-1} and a FWHM bandwidth of 1800 cm^{-1}. The nonnegative $A(t)$ was computed from $\chi^{(3)}(t)$ using Eqs. (4)–(7), with an averaging window size $w = 300$ fs, $\gamma = 2.0$, and $t_m = 2000$ fs. The pulse spectrum $\tilde{E}(\omega)$ was selected by examining 100 pulses generated by the proposed iterative method and selecting the pulse that best rejected CB. The vibrational amplitude $Q(t)$ and anti-Stokes signal $\tilde{P}^{(3)}(\omega)$ were computed using Eqs. (1) and (2). The anti-Stokes high-pass filter rejected frequencies less than 14,000 cm^{-1}.

The results are in Fig. 2. Figures 2(a) and 2(c) show that the excitation conforms to the source spectrum and the Raman spectrum of the target, with deviation from the target spectrum occurring at low fre-

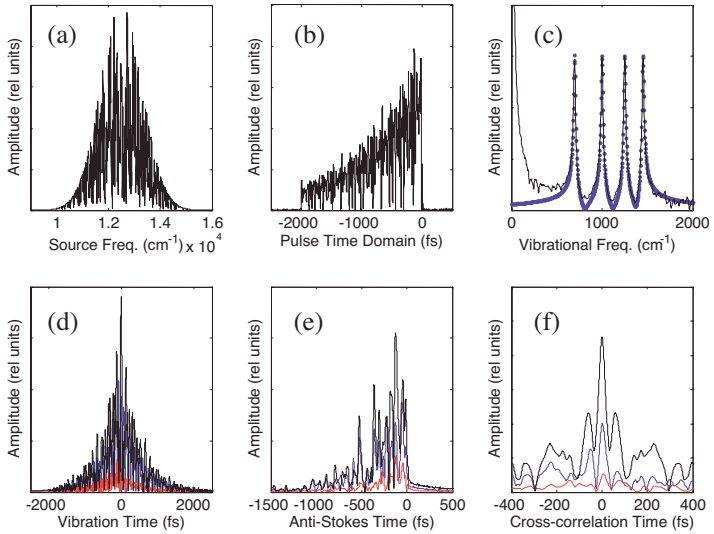

Fig. 2. Results of a simulation of matched pulse Raman excitation. (a) Spectrum of the shaped pulse. (b) Magnitude in the time domain of the shaped pulse. (c) Magnitude of the Raman spectrum of the molecule [solid black curve (blue online)] and the achieved spectrum (thin black curve) by the iterative method. (d) Amplitude of the induced total vibrational oscillation of each molecule. (e) Amplitude of the anti-Stokes signal from each molecule. (f) Amplitude of the cross correlation of the anti-Stokes signal of each molecule with the target molecule anti-Stokes signal. In (d)–(f), the upper curve (black) is of the target molecule, the lower curve (red online) for confounder A, and the middle curve (blue online) for confounder B.

quencies because of the distortion introduced by $W(t)$. Figure 2(d), the vibrational amplitude $Q(t)$ of the three molecules, shows that at $t=0$ the greatest amplitude occurs for the target molecule (thin black curve) as expected. Less polarization is generated for CB and little occurs for CA. Figure 2(e) shows the anti-Stokes signal $P^{(3)}(t)$ scattered by each molecule after the high-pass filter. Because the anti-Stokes power is proportional to molecular concentration squared, the relevant quantity for distinguishing the concentration of a target from a confounder is $\sqrt{P/P_T}$, where P and P_T are the power emitted by a confounder and the target, respectively, at the same concentration. This ratio $\sqrt{P/P_T}$ for CA is 0.204 and for CB is 0.622. Finally, Fig. 2(f) is the cross correlation $\Delta I(\Delta t)$ between the anti-Stokes signal of each molecule and the target molecule. At $\Delta t=0$, the cross-correlation amplitude relative to the target of CA is 0.104 and CB is 0.438, so that interferometry rejects the confounders better than power measurements, because interferometry utilizes the temporal shape of the anti-Stokes signal.

To assess performance, we compare the relative amplitudes of the anti-Stokes cross correlations to the cross correlations of the Raman susceptibilities given by

$$\rho = \left| \frac{\int_{-\infty}^{\infty} dt \chi_C(t)\chi_T(t)}{\int_{-\infty}^{\infty} dt \chi_T^2(t)} \right|, \tag{9}$$

where $\chi_C(t)$ and $\chi_T(t)$ are the Raman impulses of a confounder and the target, respectively. The ratio ρ characterizes how a linear matched filter separates two signals and is a reasonable estimate of the potential performance of a matched pulse. For CA, $\rho_A = 0.041$, and for CB, $\rho_B = 0.511$. Because we chose a pulse to reject CB, the matched-pulse selectivity 0.438 is slightly better than the ρ_B estimate.

Matched-pulse Raman spectroscopy is a way to identify molecules by driving the motions of normal modes into coherence, the dynamics of which are largely unexploited by conventional Raman scattering techniques. For this reason, nonlinear spectroscopy and microscopy are likely to be enhanced by exploiting coherences between molecular vibrations.

We acknowledge the scientific contributions and advice from Zhi Jiang, Wladimir Benalcazar, and Martin Gruebele from the University of Illinois at Urbana-Champaign. This research was supported in part by the National Institutes of Health (NIH) National Cancer Institute R21CA115536 and National Institute of Biomedical Imaging and Bioengineering R01EB005221, the National Science Foundation (NSF) Chemical, Bioengineering, Environment, and Transport Systems Division 0619257, and the Beckman Institute for Advanced Science and Technology.

References

1. M. D. Duncan, J. Reintjes, and T. J. Manuccia, Opt. Lett. **7**, 350 (1982).
2. J.-X. Cheng, A. Volkmer, and X. S. Xie, J. Opt. Soc. Am. B **19**, 1363 (2002).
3. D. L. Marks and S. A. Boppart, Phys. Rev. Lett. **92**, 123905 (2004).
4. G. W. Jones, D. L. Marks, C. Vinegoni, and S. A. Boppart, Opt. Lett. **31**, 1543 (2006).
5. D. L. Marks, C. Vinegoni, J. S. Bredfeldt, and S. A. Boppart, Appl. Phys. Lett. **85**, 5787 (2004).
6. J. S. Bredfeldt, C. Vinegoni, D. L. Marks, and S. A. Boppart, Opt. Lett. **30**, 495 (2005).
7. D. Oron, N. Dudovich, D. Yelin, and Y. Silberberg, Phys. Rev. Lett. **88**, 063004 (2002).
8. D. Oron, N. Dudovich, D. Yelin, and Y. Silberberg, Phys. Rev. A **65**, 043408 (2002).
9. R. E. Blahut, *Theory of Remote Image Formation* (Cambridge U. Press, 2004).
10. A. M. Weiner, Rev. Sci. Instrum. **71**, 1929 (2000).